NASA/TM-2011-216156

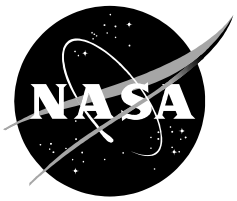

The Conditional Equivalence of ΔV Minimization and Apoapsis Targeting in Numerical Predictor-Corrector Aerocapture Guidance

Jarret M. Lafleur

NASA Johnson Space Center, Houston

National Aeronautics and
Space Administration

Lyndon B. Johnson Space Center
Houston, Texas 77058

August 2011

The NASA STI Program Office . . . in Profile

Since its founding, NASA has been dedicated to the advancement of aeronautics and space science. The NASA Scientific and Technical Information (STI) Program Office plays a key part in helping NASA maintain this important role.

The NASA STI Program Office is operated by Langley Research Center, the lead center for NASA's scientific and technical information. The NASA STI Program Office provides access to the NASA STI Database, the largest collection of aeronautical and space science STI in the world. The Program Office is also NASA's institutional mechanism for disseminating the results of its research and development activities. These results are published by NASA in the NASA STI Report Series, which includes the following report types:

- TECHNICAL PUBLICATION. Reports of completed research or a major significant phase of research that present the results of NASA programs and include extensive data or theoretical analysis. Includes compilations of significant scientific and technical data and information deemed to be of continuing reference value. NASA's counterpart of peer-reviewed formal professional papers but has less stringent limitations on manuscript length and extent of graphic presentations.
- TECHNICAL MEMORANDUM. Scientific and technical findings that are preliminary or of specialized interest, e.g., quick release reports, working papers, and bibliographies that contain minimal annotation. Does not contain extensive analysis.
- CONTRACTOR REPORT. Scientific and technical findings by NASA-sponsored contractors and grantees.
- CONFERENCE PUBLICATION. Collected papers from scientific and technical conferences, symposia, seminars, or other meetings sponsored or cosponsored by NASA.
- SPECIAL PUBLICATION. Scientific, technical, or historical information from NASA programs, projects, and mission, often concerned with subjects having substantial public interest.
- TECHNICAL TRANSLATION English-language translations of foreign scientific and technical material pertinent to NASA's mission.

Specialized services that complement the STI Program Office's diverse offerings include creating custom thesauri, building customized databases, organizing and publishing research results . . . even providing videos.

For more information about the NASA STI Program Office, see the following:

- Access the NASA STI Program Home Page at http://www.sti.nasa.gov
- E-mail your question via the Internet to help@sti.nasa.gov
- Fax your question to the NASA Access Help Desk at (301) 621-0134
- Telephone the NASA Access Help Desk at (301) 621-0390
- Write to:
  NASA Access Help Desk
  NASA Center for AeroSpace Information
  7115 Standard
  Hanover, MD 21076-1320

NASA/TM-2011-216156

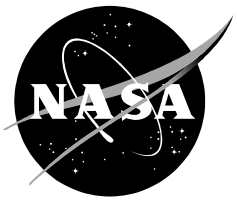

The Conditional Equivalence of ΔV Minimization and Apoapsis Targeting in Numerical Predictor-Corrector Aerocapture Guidance

Jarret M. Lafleur

NASA Johnson Space Center, Houston

National Aeronautics and
Space Administration

Lyndon B. Johnson Space Center
Houston, Texas 77058

August 2011

Acknowledgments

This work would not have been possible without the guidance and support of Chris Cerimele, Lee Bryant, Jeremy Rea, Ron Sostaric, Mark Orr, Mike Tigges, Tim Crull, Carlie Zumwalt, and Dan Matz in the Aeroscience and Flight Mechanics Division at NASA Johnson Space Center. Thanks are also due to Jody Mantell and Ellen Howard at the University of Houston Clear Lake Neumann Library for locating many of the references cited in this paper.

Available from:

NASA Center for AeroSpace Information
7115 Standard Drive
Hanover, MD 21076-1320
301-621-0390

National Technical Information Service
5285 Port Royal Road
Springfield, VA 22161
703-605-6000

This report is also available in electronic form at http://ston.jsc.nasa.gov/collections/TRS/

Abstract

Interest in aerocapture, a maneuver in which a spacecraft dives into the atmosphere of a planet for nearly propellantless capture into planetary orbit, has grown steadily in recent years. One key element required to execute this maneuver is an appropriate guidance algorithm for the atmospheric phase of flight. A popular algorithm choice has been the numerical-predictor corrector (NPC), which typically iterates on a time-invariant bank angle to target apoapsis of the desired final orbit. This paper introduces the idea of using the NPC to select the bank angle that instead minimizes the sum of periapsis-raise ΔV and apoapsis-cleanup ΔV, and demonstrates the surprising finding that the two approaches are equivalent under a certain analytic condition. This condition is derived and then applied to correctly predict a scenario in which apoapsis targeting produces a suboptimal ΔV. This scenario is simulated, and the ΔV minimization algorithm is shown to reduce the required ΔV by 23%. Monte Carlo simulations confirm both the scenarios of equivalence and non-equivalence, and an automatable procedure is outlined that a user can execute prior to simulating or flying a trajectory to determine whether apoapsis targeting is ΔV optimal or whether a ΔV minimization algorithm is required.

Contents

Figures

Tables

Acronyms

AFE	aeroassist flight experiment
ΔV	orbital velocity change
ΔV_1	orbital velocity change to raise periapsis
ΔV_2	orbital velocity change to zero apoapsis error
GRAM	Global Reference Atmosphere Model
ISPT	In-space Propulsion Technology (Project)
L/D	lift-to-drag ratio
LEO	low-Earth orbit
μ	planet-specific gravitational constant
NPC	numeric predictor-corrector
1-D	one-dimensional
r_a	post-aerocapture apoapsis radius
r_{aT}	target orbit apoapsis radius
r_p	post-aerocapture periapsis radius
r_{pT}	target orbit periapsis radius
φ	bank angle
SORT	Simulation to Optimize Rocket Trajectories

1. Introduction

Over the past decade, a consistent theme among studies for advanced robotic and human interplanetary missions has been the use of aerocapture to achieve planetary orbit insertion. In the aerocapture maneuver, an arriving spacecraft dives into the atmosphere of a planet to aerodynamically dissipate excess kinetic energy and capture into a target orbit. The advantage is the near elimination of the need to carry propellant for orbit insertion. For robotic missions, this can translate into hundreds of kilograms of mass reduction, which in turn permits spacecraft to carry greater payload, launch on a less-costly launch vehicle, or reduce transit time.[1,2]

Interest in aerocapture has grown steadily in recent years. Since 2002, the NASA In-Space Propulsion Technology (ISPT) Project, funded by the NASA Science Mission Directorate, has devoted resources to developing technologies and techniques that will allow aerocapture to be demonstrated and validated in flight.[1,3] A system study sponsored by the ISPT Project in 2003 demonstrated that aerocapture enables certain robotic missions to Neptune, Saturn, and Jupiter that would be unachievable by traditional means, and that it allows the delivery of up to 280% more mass to other candidate destinations in the solar system.[4] In 2006, the NASA Solar System Exploration Roadmap identified aerocapture technologies and flight validation as a high priority, particularly since they would enable two candidate flagship-class outer planet missions.[3,5]

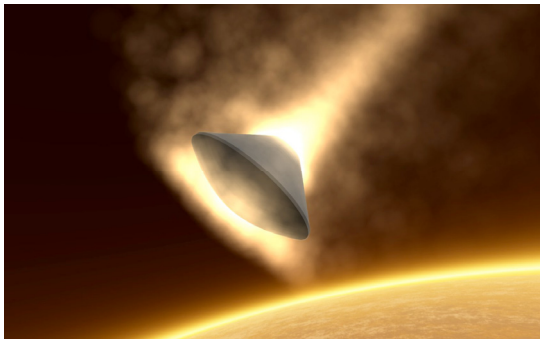

Figure 1. Artist's concept of Mars aerocapture.[13]

Outside the realm of robotic exploration, the most recent NASA Mars Design Reference Architecture 5.0 uses aerocapture for the deceleration of cargo-carrying landers on Mars arrival,[6] and the technique has been assumed in numerous previous human Mars landing architecture studies.[7-11] Most recently, the NASA Office of the Chief Technologist has identified aerocapture as a potential crosscutting technology demonstration (fig. 1) for its new system-level Technology Demonstration Missions Program.[12,13]

One key element to successful aerocapture is sufficient guidance during the maneuver.[3] During aerocapture, a spacecraft must typically modulate its bank angle and thus rotate its lift vector to respond to dispersions, thereby ensuring that it reaches its target orbit after atmospheric exit. A variety of aerocapture guidance algorithms have been proposed over the past few decades (e.g., see the surveys of Refs. 14-15 and Refs. 16-26), although a popular choice for flight program proposals over the past two decades has been the Draper Laboratory PredGuid numeric predictor-corrector algorithm.[2,17,27-32] When the PredGuid algorithm is called to command a bank angle at any point in a trajectory, it quickly iterates over the range of possible [time-invariant] bank angles to find the precise bank angle that allows the vehicle to achieve its targeted apoapsis at the end of the trajectory. At each iteration (i.e., for each bank angle guess), the achieved apoapsis is predicted by numerically integrating equations of motion; hence PredGuid is classified as a numeric predictor-corrector (NPC).

This paper explores a basic question that arises in even the brief discussion of PredGuid above: Why target apoapsis? Although the minimization of apoapsis error is desired, it is desired because it is correlated with minimization of the ΔV needed to correct from the post-aerocapture orbit to the final desired orbit. However, when targeting apoapsis, it is possible that guidance will

select a bank angle that improves error in apoapsis at the expense of error in periapsis, resulting in a ΔV (and, therefore, vehicle mass) that is greater than necessary.

The idea of targeting apoapsis is common among aerocapture guidance algorithms (in addition to PredGuid, see also Refs. 19-20). As a result, the discussion in this paper may be broadly relevant for future aerocapture guidance development. In the case of PredGuid and similar NPCs, this paper will show that, as expected, a guidance based on ΔV minimization is more ΔV-optimal than one that is based on apoapsis targeting. However, importantly (and non-intuitively), under a certain analytic inequality condition – which may be met in a wide range of scenarios – the two are theoretically identical.

1.1 Aerocapture Phases and ΔV Maneuvers

Figure 2 depicts the sequence of aerocapture events and the definition of ΔV events commonly used in aerocapture studies. Starting on the left, an incoming vehicle arrives on a high-energy (e.g., hyperbolic or high-energy elliptic) orbit in the vicinity of its target planet. Typically, aerocapture guidance activates soon after atmospheric interface and modulates bank angle while the vehicle is within the substantial atmosphere. In the planar case, the atmospheric flight phase has the effect of decreasing the orbital energy of the spacecraft as well as changing the apoapsis altitude, periapsis altitude, and line of apsides of the vehicle. All orbital elements, including inclination, can change in the full three-dimensional case (not depicted in fig. 2).

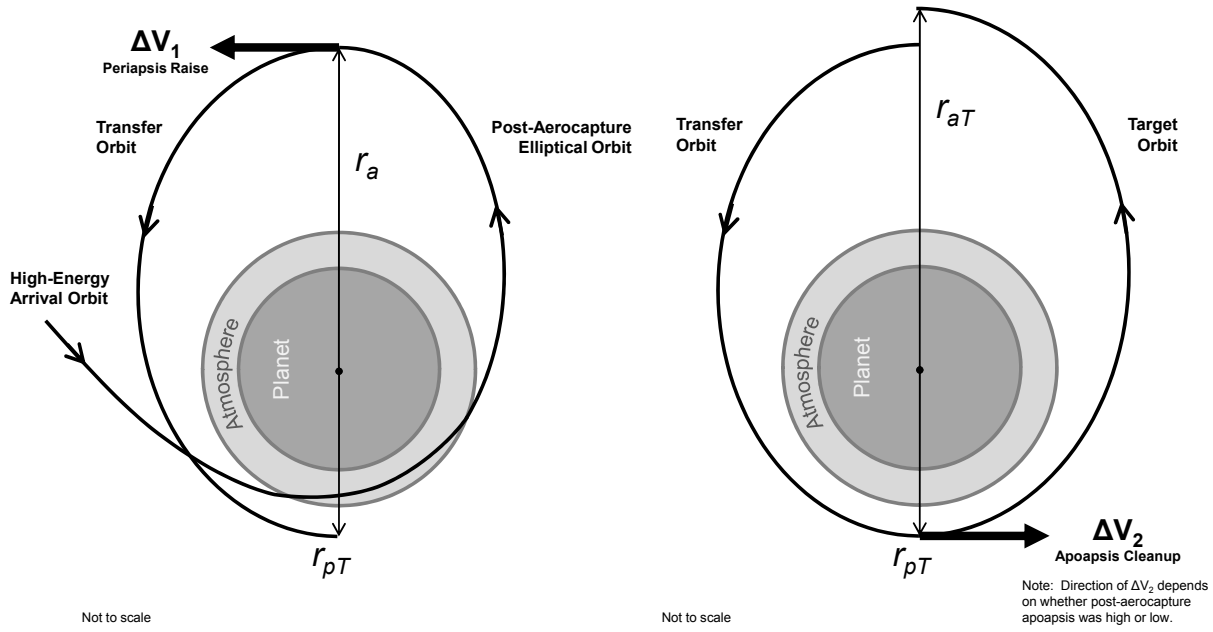

Figure 2. Post-aerocapture Hohmann transfer to target orbit (on left, periapsis raise burn; on right, apoapsis cleanup burn).

The vehicle can be modeled through simple two-body orbital mechanics on atmospheric exit. Under the assumption that orbit transfer time is a free parameter and that the vehicle uses high-thrust propulsion, the following Hohmann-like burn sequence is feasible and generally near-

optimal in terms of ΔV:* At the apoapsis (r_a) of the post-aerocapture elliptical orbit, a posigrade tangential burn (ΔV_1) is performed to raise periapsis to the desired target orbit periapsis (r_{pT}) as shown on the left in figure 2. As shown in the right half of figure 2, once the vehicle reaches its new periapsis (r_{pT}), it performs a second tangential burn (ΔV_2) to correct its apoapsis to equal the target apoapsis (r_{aT}). The direction of this second burn may be either posigrade or retrograde, depending on whether the post-aerocapture apoapsis is below or above the target apoapsis. It can be shown, via the equations of two-body orbital mechanics, that the magnitudes of ΔV_1 and ΔV_2 are described by the functions of post-aerocapture apoapsis (r_a), post-aerocapture periapsis (r_p), target orbit apoapsis (r_{aT}), and target orbit periapsis shown in Eq(1) and Eq(2). Note that μ represents the gravitational parameter of the planet. Note also that absolute value symbols are omitted from Eq(1) since perigee must always be raised (not lowered) and, thus, the apoapsis velocity of the transfer orbit must always be higher than that of the post-aerocapture orbit.

$$\Delta V_1 = \sqrt{2\mu} \cdot \left(\sqrt{\frac{1}{r_a} - \frac{1}{r_a + r_{pT}}} - \sqrt{\frac{1}{r_a}\frac{r_p}{r_a + r_p}} \right) \tag{1}$$

$$\Delta V_2 = \sqrt{2\mu} \cdot \left| \sqrt{\frac{1}{r_{pT}} - \frac{1}{r_{aT} + r_{pT}}} - \sqrt{\frac{1}{r_{pT}} - \frac{1}{r_a + r_{pT}}} \right| \tag{2}$$

1.2 PredGuid Aerocapture Guidance and Orion Lunar Return Test Case

The PredGuid aerocapture guidance algorithm used throughout this study has its origins with Higgins at the Charles Stark Draper Laboratory in 1984, and it became a leading guidance concept for the proposed 1992 launch of an aeroassist flight experiment (AFE) from the space shuttle payload bay.[17,29] In 2001, the algorithm was also included in an Aerocapture Flight Test Experiment (AFTE) proposal for the NASA New Millennium Program ST-7 technology demonstrator.[2] Although neither experiment flew, the intent of each would have been to validate aerocapture using entry conditions similar to those that would be experienced on return from a geostationary orbit. While the algorithm has been modified throughout the past few decades (e.g., see Refs. 17 and 33), its basic operation remains straightforward: Continually during aerocapture, the vehicle on-board computer numerically simulates the remainder of the trajectory and selects the bank angle it should hold to reach the proper exit condition (e.g., the target apoapsis altitude).

Most recently, the PredGuid guidance algorithm has been adapted for use in skip-entry scenarios for the NASA Orion crew exploration vehicle.[27,28,30-32] To preserve flight heritage, most of the Orion entry guidance routines are adapted from the Apollo Program (see fig. 3 for the original Apollo skip-entry guidance phases); however, the Apollo contingency skip-entry capability produces unacceptably large landing location dispersions (amounting to hundreds of

*Because this sequence raises periapsis before correcting apoapsis, it is not necessarily ΔV-optimal. In some instances, less ΔV may be required if an apoapsis cleanup burn is performed as soon as the vehicle leaves the atmosphere, followed by the periapsis raise burn when the vehicle arrives at apoapsis. However, such a sequence is not always optimal, has a less straightforward ΔV computation, and poses the practical difficulty to the operator of performing a precise burn perhaps just a few minutes after the aerocapture maneuver.

kilometers in the 99.7th percentile[30]) when used to guide the vehicle to a target that is more than about 2700 nmi (5000 km) downrange.[30] This problem was new to Orion, which was required to make a precision landing at a continental U.S. target as many as 5400 nmi (10 000 km) down-range (corresponding to worst-case lunar return phasing).[30] The solution NASA selected was to use PredGuid to replace the down control, up control, and ballistic guidance phases of the original Apollo guidance (see fig. 3).[30,31]

The version of PredGuid used in the present study is *PredGuid+A*, which is an enhanced version of this most recent PredGuid implementation that is written in C and readapted for aerocapture applications. Modifications and enhancements include the following:

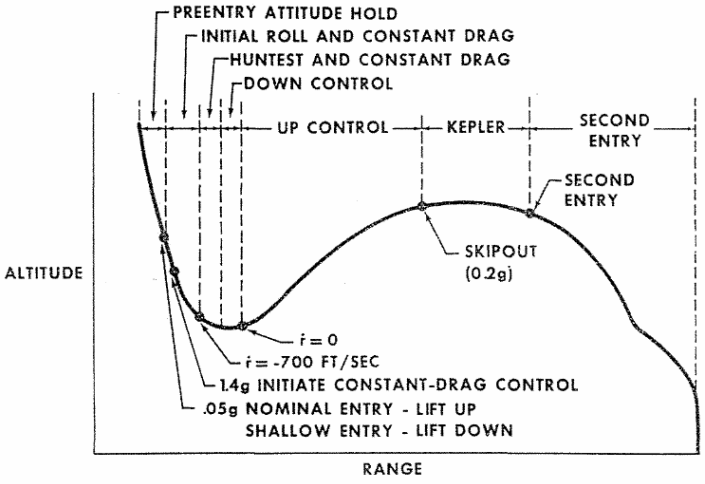

Figure 3. Original Apollo skip-entry guidance phases.[30]

- The PredGuid C code has been interfaced with the NASA Johnson Space Center FORTRAN-based Simulation to Optimize Rocket Trajectories (SORT).[34]
- A new operational mode (Mode 6) allows the user to designate an apoapsis altitude target rather than a target landing site. The Newtonian iteration logic of the PredGuid predictor-corrector is left unchanged, and the quantity calculated and passed to the corrector at each iteration is the predicted apoapsis altitude of the vehicle instead of the predicted range at simulation termination. This apoapsis is predicted based on two-body orbital elements calculated from the position and velocity vectors at simulation termination (e.g., at a 600 000-ft (182.9-km)-altitude atmospheric exit).
- An additional operational mode (Mode 7) allows the user to designate a target final orbit in terms of apoapsis and periapsis altitude. In this mode, *PredGuid+A* uses a golden section one-dimensional line search algorithm to select the bank angle that minimizes the sum of the ΔV values in Eq(1) and Eq(2). As in Mode 6, the apoapsis and periapsis radii required for Eq(1) and Eq(2) are computed based on two-body orbital elements from the vehicle position and velocity vectors at simulation termination. Differences between Mode 7 and Mode 6 are the primary subject of the present paper.
- The conditions for transitioning between guidance phases (i.e., the phases in Fig. 3) for the new aerocapture modes are nearly identical to those of Mode 3 (the standard mode for Orion lunar return skip entry, which uses the PredGuid NPC during the down control, up control, and ballistic phases in fig. 3). The main exception to this is a new constraint that requires an entering hyperbolic vehicle to remain in the Apollo constant-drag phase until orbital energy is negative. This stems from the observation that apoapsis radii predicted by the NPC for hyperbolically entering vehicles can be negative, which would incorrectly be interpreted as a "low" miss.[29]
- A second, minor phase transition modification for the aerocapture modes allows up control to begin once the sensible atmospheric drag is reached (and once the vehicle is no longer on a hyperbolic trajectory). To enable this and avoid the need to set a separate constant (normally

known as Q7) for the start of up control, the Q7 constant for aerocapture modes is set to the PredGuid current default sensible atmospheric drag level (1.6 ft/s^2 [0.5 m/s^2], or 0.05g). Entry into huntest phase from the initial roll phase is also no longer restricted by an altitude rate requirement of 700 fps (213.4 m/s), as it is in the Apollo algorithm.

- The target plane for the lateral logic, which selects whether to bank to port or starboard once the NPC has chosen the proper cosine of the bank angle, has also been modified. The skip-entry algorithm lateral logic previously attempted to align the trajectory plane of the vehicle (defined by the Earth-centric position vector and inertial velocity of the vehicle) with the plane containing the vehicle, landing site, and center of the Earth. In contrast, the aerocapture implementation (Modes 6 and 7) attempts to maintain the initial trajectory plane of the vehicle. In addition, the new implementation avoids the use of a small angle assumption that existed in the original code.[35]
- Above 400 000 ft (122 km) in altitude, the assumed atmospheric density profile of PredGuid is now set identical to the SORT 1976 U.S. Standard Atmosphere model. Previously, the two showed sharp disagreement above 400 000 ft (122 km) when viewed on a semilogarithmic plot, with the previous PredGuid model exhibiting a slope (C^1) discontinuity at 400 000 ft (122 km).
- Finally, the typical Orion lift-to-drag ratio (L/D) estimation bias of 0.90 is changed to 1.00 to allow the vehicle to more effectively use its L/D capability and to allow the predictor to more accurately estimate the vehicle atmospheric exit conditions.

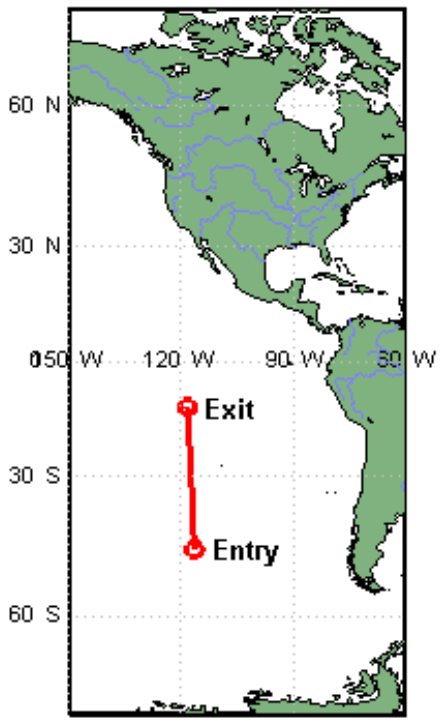

Figure 4. Representative ground track for Orion lunar return aerocapture into LEO.

As a result of these modifications, the same PredGuid code previously used for Orion skip-entry can also be used for aerocapture once the user changes the input mode (to 6 or 7) and inputs a target apoapsis (and, if applicable, periapsis) altitude. As an example of the ease with which this mode can be changed, this paper applies the new aerocapture capability to an Orion lunar return test case; once PredGuid commands the up-control phase, the vehicle now simply uses the NPC to target an apoapsis or minimize ΔV instead of targeting a range.

The Orion lunar return case, with initial conditions similar in altitude, speed, and flight path angle to those of Ref. 35 and the verification case of Ref. 30, enters Earth's atmosphere while headed north over the South Pacific Ocean, 4770 nmi (8840 km) distant from the normal Orion San Clemente landing target. Figure 4 illustrates this entry location as well as a representative ground track for aerocapture into a low-Earth orbit (LEO). Note that in this study, entry and activation of the guidance is defined to occur at 400 000 ft (121.9 km) altitude, but exit is defined at the 600 000-ft (182.9-km) upper extent of the PredGuid 1976 U.S. Standard Atmosphere model, which provides additional confidence in the drag-free two-body apoapsis calculation described earlier.

The full entry state for the test case is specified in Table 1. The assumed mass of the Orion capsule is 19 805 lbm (8983 kg), and the hypersonic L/D is 0.27, with a hypersonic drag coefficient of 1.37 and a reference area of 213.8 ft^2 (19.86 m^2). Mach-dependent aerodynamics are modeled. Also, during flight, SORT limits bank rate to 15 deg/s, limits bank acceleration to 5 deg/s^2, and imposes a bank angle deadband of 1.0 deg.

Table 1. Initial State for Orion Lunar Return Test Case

Initial Position			Initial Velocity		
Geodetic Altitude	400 000 ft	(121.9 km)	Inertial Velocity	36 150 fps	(11.02 km/s)
Geodetic Latitude	46.66992°S		Inertial Flight Path Angle	-5.91 deg	
Longitude	116.5°W		Inertial Azimuth	0 deg	

2. Empirical Observation: Equivalence of Apoapsis Targeting and ΔV Minimization

As described in Section 1.2., *PredGuid+A* has the capability to either (1) target the apoapsis altitude of the post-aerocapture orbit; or (2) attempt to minimize the ΔV required to maneuver from the post-aerocapture orbit to the final target orbit (as defined by Eqs[1] and Eq[2]). The former capability is the more traditional means of guidance targeting and tends to be correlated with ΔV minimization, while the latter capability effects ΔV minimization directly. An empirical comparison of these two methods follows, and a noteworthy observation is made.

Figure 5 shows data from a sample aerocapture trajectory using the initial conditions of Table 1 and targeting an apoapsis altitude of 229 nmi (425 km). The top left plot shows the commanded and actual bank angle histories; as shown, the vehicle remains in the Apollo initial roll phase (at a -15-deg bank angle, the maximum allowed to prevent saturation) for the first 30 sec of the trajectory. Once the 1.6 ft/s^2 (0.5 m/s^2) sensible atmospheric drag threshold is crossed, the NPC becomes active, commanding a bank angle of -40.4 deg. *PredGuid+A* commands this particular bank angle because its internal predictor finds that this angle will allow the vehicle to hit the 230-nmi (426-km) apoapsis altitude target; the fact that this bank angle remains relatively constant for nearly one minute indicates good agreement between the *PredGuid+A* internal predictor simulation and the actual SORT simulation conditions (which are different, for example, because *PredGuid+A* does not simulate bank reversals; Mach-dependent aerodynamics; J3 or J4 effects; or bank rate, acceleration, and deadband limits).

About 1:26 into the trajectory, the sign of the bank angle is flipped since the vehicle exceeds its lateral corridor and must execute a bank reversal. This new bank angle of similar magnitude but opposite sign is maintained for another 32 sec until the next bank reversal, after which relatively little control authority remains and the NPC eventually again commands the maximum-lift -15-deg bank angle. The NPC deactivates at 3:15 when the 1.6 ft/s^2 (0.5 m/s^2) threshold is crossed again, and the previous bank angle is maintained for the remainder of the trajectory. Calculation of the two-body orbital elements at the end of the trajectory (at 7:29; not shown on these plots) shows that the vehicle hits its apoapsis target altitude to within 900 ft (270 m).

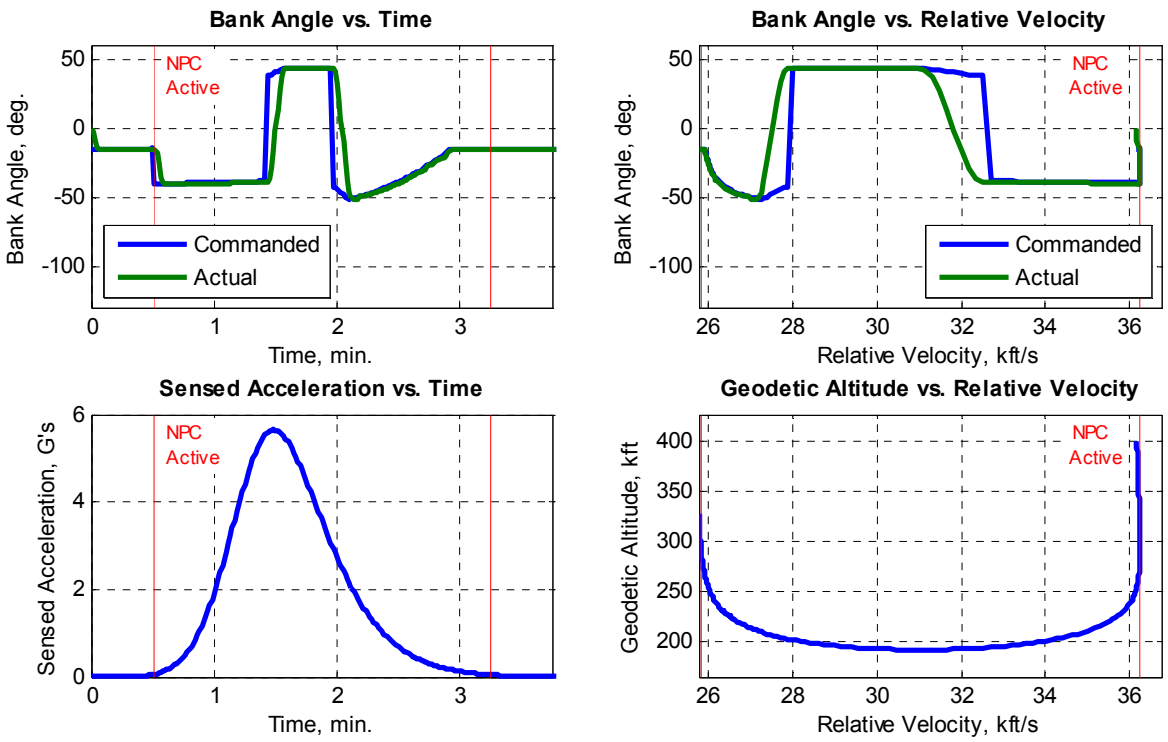

Figure 5. Nominal aerocapture trajectory to 229 nmi (425 km) LEO using apoapsis targeting.

Figure 6 shows data from a sample aerocapture trajectory with initial conditions identical to those of figure 5 but using *PredGuid+A* in its ΔV minimization mode for a target circular orbit of 229 nmi (425 km). With the exception of a bank angle drift starting at 2:38 (at which point very little control authority remains, and the exit conditions are difficult to change),[†] the trajectory profiles are nearly identical. This is emphasized in figure 7, which overlays the commanded bank angle plots from figures 5 and 6. The two trajectories are so similar that the final two-body ΔV computations agree within 3.7 fps (1.1 m/s).

Why should both ΔV minimization and apoapsis targeting, two entirely separate methods for choosing bank angle, produce nearly identical results? That this should happen is not intuitive.

To investigate empirically, we consider apoapsis targeting as a starting point. At any call of the guidance between 0:31 and 3:15, the NPC chooses the bank angle that produces the correct final apoapsis altitude if the angle is held constant throughout the remainder of the flight. As noted earlier, for apoapsis targeting, the NPC initially chooses a bank angle of -40.4 deg. This also happens to be ΔV optimal because, for example, if it had chosen -40.3 deg (slightly more lift-up), the apoapsis cleanup burn (ΔV_2) would have increased by 6.8 fps (2.1 m/s) since apoapsis would have been missed and the savings in the periapsis raise burn (ΔV_1) would only have been 4.6 fps (1.4 m/s). If it had chosen -40.5 deg, both ΔV values would have increased. As a result, because of the relative trades between ΔV_1 and ΔV_2, this bank angle solution is also locally the minimum ΔV solution. However, this is not the case for all scenarios.

[†]While it produces a negligible impact on exit conditions, the cause for this difference in drift tendency late in the trajectory is not yet fully explained. It may, however, be hypothesized that slight bank angle differences early in the trajectory impact the direction of the final apoapsis miss, from missing low (and requiring full lift up) for the apoapsis targeting case to missing high (and trending toward full lift down) for the ΔV minimization case.

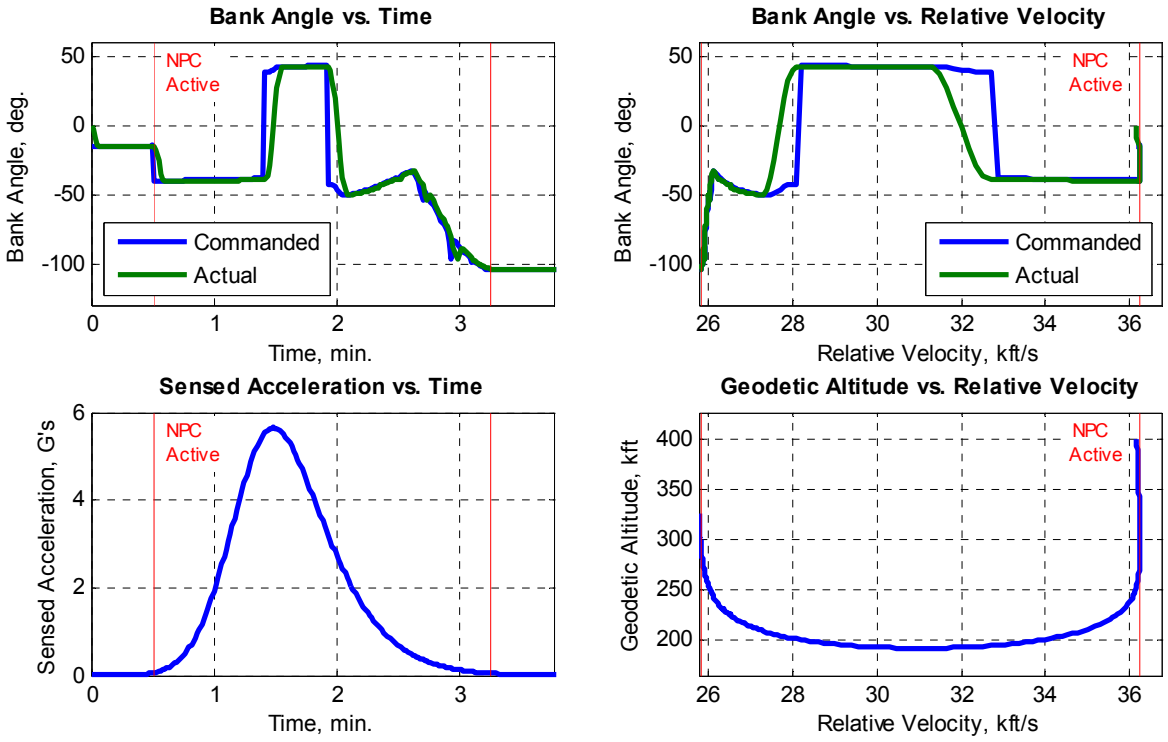

Figure 6. Nominal aerocapture trajectory to 229 nmi (425 km) LEO using ΔV minimization.

3. Analytical Condition of Equivalence

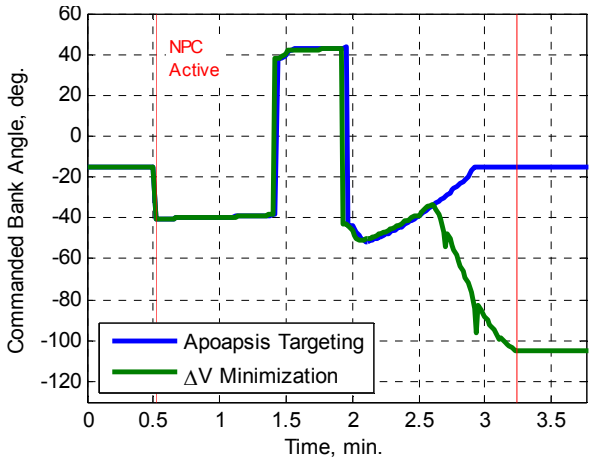

Figure 7. Comparison of commanded bank angle between apoapsis targeting and ΔV minimization methods.

The empirical equivalence observed in Section 2 is not a coincidence, but is an analytical consequence of Eq(1) and Eq(2) as well as the apoapsis and periapsis trades available to the NPC as it iterates on the bank angle. This section investigates these analytics and identifies the condition that must be met to result in an apoapsis targeting identical to ΔV minimization. Importantly, this condition will also allow us to identify (and then test) scenarios in which apoapsis targeting and ΔV minimization are *not* identical and, thus, where the ΔV minimization technique can result in significant propellant savings.

Figure 8 plots the predicted final apoapsis and periapsis altitudes as a function of bank angle that are visible to the NPC once it activates 31 sec into the trajectory of figures 5 and 6. In apoapsis targeting, the NPC would ignore the lower plot and select $\varphi = 40.4$ deg (the sign of the angle is chosen later by the lateral logic) because it achieves the desired final apoapsis altitude of 229 nmi (425 km). If it had chosen a lower bank angle, the vehicle would have skipped out of the

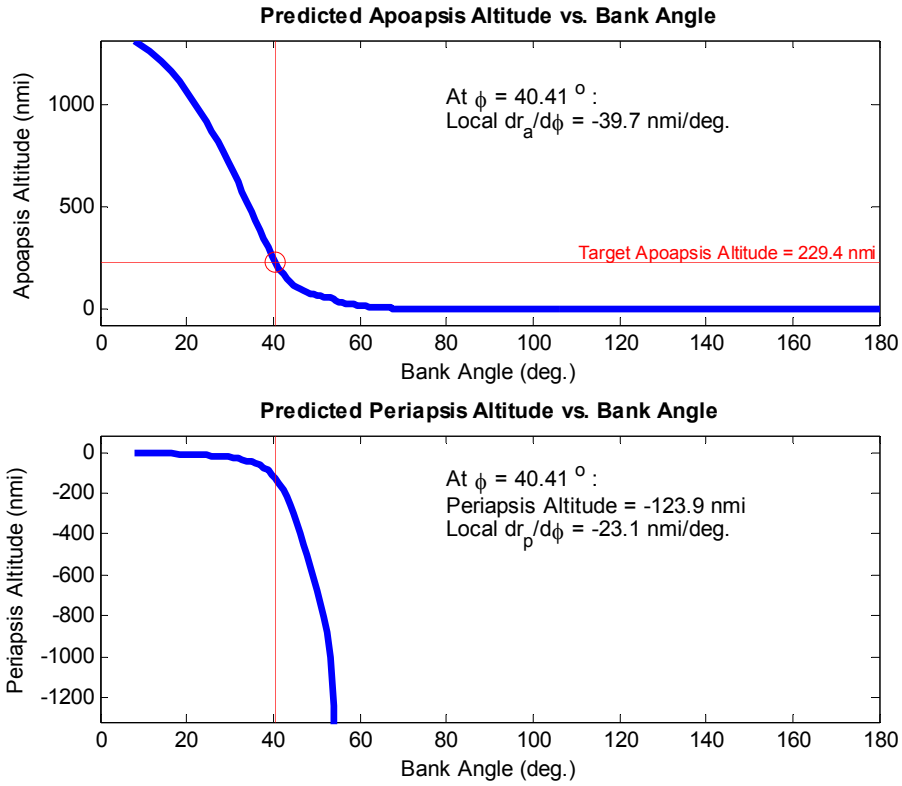

Figure 8. Apoapsis and periapsis altitude curves visible to the NPC at 0:31.

atmosphere earlier, and apoapsis would have been too high. If it had chosen a higher bank angle, the vehicle would have dived deeper into the atmosphere and have dissipated more energy, making apoapsis too low.[‡] Locally near φ = 40.4 deg, the upper plot of figure 8 shows that for every 1 deg increase in bank angle, achieved apoapsis altitude is lowered by 39.7 nmi (73.5 km).

The lower plot of figure 8 becomes important for computation of ΔV as defined in Eq(1) and Eq(2). First, note that not only is simultaneous targeting of a 229-nmi (425-km) apoapsis and 229-nmi (425-km) periapsis impossible, but targeting even a positive periapsis altitude is impossible (all points on this line have negative y-axis values). If apoapsis altitude is targeted with φ = 40.4 deg, the achieved periapsis altitude is predicted to be -123.9 nmi (-229.5 km). Locally near φ = 40.4 deg, for every 1-deg increase bank angle, achieved periapsis altitude is lowered by 23.1 nmi (42.8 km).

This leads to two important observations. First, it is clearly not ΔV-favorable to increase bank angle beyond 40.4 deg, since there will exist an apoapsis error *and* periapsis error will increase. This would be true regardless of the relative magnitudes of the apoapsis and periapsis derivatives, provided both are negative. Second, if the opposite change (a decrease) in bank angle is considered, a trade is involved: Every degree of decrease in bank angle will [locally] improve periapsis error by 23.1 nmi (42.8 km) but degrade apoapsis error by 39.7 nmi (73.5 km). This suggests that such a trade may not be worthwhile (and that targeting apoapsis may indeed be ΔV-optimal), but this must be examined more thoroughly because total ΔV is not equally sensitive to periapsis and apoapsis altitude changes.

3.1 Derivation

To investigate the hypothesis that moving slightly to the left in bank angle in figure 8 is suboptimal, we start with the recognition that total ΔV is given by Eq(3), where ΔV_1 and ΔV_2 are given by Eq(1) and Eq(2). Differentiating with respect to bank angle φ yields Eq(4).

[‡]In this particular example, trajectories with bank angles above about 64 deg terminate in the vehicle impacting the surface of the Earth rather than skipping out of the atmosphere.

$$\Delta V = \Delta V_1 + \Delta V_2 \tag{3}$$

$$\frac{d(\Delta V)}{d\phi} = \frac{d(\Delta V_1)}{d\phi} + \frac{d(\Delta V_2)}{d\phi} \tag{4}$$

Next, in Eq(5) we note that by the chain rule the derivative of either ΔV_1 or ΔV_2 (represented generically by ΔV_x) with respect to bank angle can be expressed in terms of four derivatives. Two of these derivatives, $dr_a/d\varphi$ and $dr_p/d\varphi$, have already been recorded in figure 8. These derivatives describe locally how apoapsis and periapsis altitudes vary with the NPC choice of bank angle.

$$\frac{d(\Delta V_x)}{d\phi} = \frac{\partial(\Delta V_x)}{\partial r_a}\frac{dr_a}{d\phi} + \frac{\partial(\Delta V_x)}{\partial r_p}\frac{dr_p}{d\phi} \tag{5}$$

The other derivatives in Eq(5) can be computed analytically from Eq(1) and Eq(2), and are given by Eq(6) through Eq(9) below (after considerable simplification). Equation (8) accounts for the special fact that the derivative is to be evaluated where $r_a = r_{aT}$ (i.e., where $\Delta V_2 = 0$), and ΔV_2 can only increase if r_a is changed from r_{aT}. Also, recall that the target orbit apoapsis and periapsis (r_{aT} and r_{pT}, respectively) are constants for any given problem.

$$\frac{\partial(\Delta V_1)}{\partial r_a} = \frac{\sqrt{2\mu}}{2}\left[\sqrt{r_p}\,\frac{2r_a + r_p}{\left(r_a^2 + r_p r_a\right)^{3/2}} - \sqrt{r_{pT}}\,\frac{2r_a + r_{pT}}{\left(r_a^2 + r_{pT} r_a\right)^{3/2}}\right] \tag{6}$$

$$\frac{\partial(\Delta V_1)}{\partial r_p} = -\frac{\sqrt{2\mu}}{2\left(r_a + r_p\right)^{3/2}}\sqrt{\frac{r_a}{r_p}} \tag{7}$$

$$\frac{\partial(\Delta V_2)}{\partial r_a} = \begin{cases} -\dfrac{\sqrt{2\mu}}{2}\dfrac{\sqrt{r_{pT}}}{\sqrt{r_a}\left(r_a + r_{pT}\right)^{3/2}}, & r_a < r_{aT} \\ \dfrac{\sqrt{2\mu}}{2}\dfrac{\sqrt{r_{pT}}}{\sqrt{r_a}\left(r_a + r_{pT}\right)^{3/2}}, & r_a > r_{aT} \end{cases} \tag{8}$$

$$\frac{\partial(\Delta V_2)}{\partial r_p} = 0 \tag{9}$$

Now, for ΔV minimization to produce any benefit over apoapsis targeting, apoapsis targeting must not already be a ΔV minimum. *If both apoapsis and periapsis altitudes are monotonically decreasing functions of bank angle*, then, as observed earlier, increasing bank angle past the apoapsis target angle cannot be ΔV-optimal since both periapsis and apoapsis errors increase. If bank angle is decreased, it will result in a ΔV benefit only if the increase in the apoapsis cleanup

maneuver (ΔV_2) is offset by the decrease in periapsis raise maneuver (ΔV_1). Conversely, this implies that *if Eq(10) is fulfilled when evaluated at* $r_a = r_{aT}$*, then apoapsis targeting and ΔV minimization are equivalent*:

$$\frac{d(\Delta V_1)}{-d\phi} + \frac{d(\Delta V_2)}{-d\phi} > 0 \tag{10}$$

The negative $d\varphi$ denominator exists to indicate that the derivative is taken for decreasing φ only. An equivalent statement is in Eq(11):

$$\frac{d(\Delta V_1)}{d\phi} < -\frac{d(\Delta V_2)}{d\phi} \tag{11}$$

Expanding Eq(11) based on the chain rule of Eq(5) yields:

$$\frac{\partial(\Delta V_1)}{\partial r_a}\frac{dr_a}{d\phi} + \frac{\partial(\Delta V_1)}{\partial r_p}\frac{dr_p}{d\phi} < -\frac{\partial(\Delta V_2)}{\partial r_a}\frac{dr_a}{d\phi} - \frac{\partial(\Delta V_2)}{\partial r_p}\frac{dr_p}{d\phi} \tag{12}$$

At this point, the analytic derivatives of Eq(6) through Eq(9) and the numeric derivatives (e.g., from fig. 8) may be plugged in and tested. Values for the Orion test case of Section 2 are given in Table 2. Note that when these values are plugged into Eq(12), the left side equals 0.0077 nmi/deg-s and the right side equals 0.0112 nmi/deg-s. *The right side is greater than the left side and the equivalence condition is fulfilled, explaining why both the apoapsis targeting and ΔV minimization techniques produce the same bank angle command in the empirical observations of Section 2*.

Table 2. Values for Testing the Equivalence Condition (cf. Eq[12]) on the Orion Lunar Return Test Case

Scenario Inputs		Derivatives	
Target Apoapsis (r_{aT})	3673.3 nmi (6803.0 km)	$dr_a/d\varphi$	-39.7 nmi/deg (-73.5 km/deg)
Target Periapsis (r_{pT})	3673.3 nmi (6803.0 km)	$dr_p/d\varphi$	-23.1 nmi/deg (-42.8 km/deg)
Selected Bank Angle (φ)	40.41°	$\partial(\Delta V_1)/\partial r_a$	-7.75×10^{-6} s^{-1}
Post-aerocapture Apoapsis (r_a)	3673.3 nmi (6803.0 km)	$\partial(\Delta V_1)/\partial r_p$	-3.19×10^{-4} s^{-1}
Post-aerocapture Periapsis (r_p)	3320.0 nmi (6148.6 km)	$\partial(\Delta V_2)/\partial r_a$	2.81×10^{-4} s^{-1}
Gravitational Parameter (μ)	62 750 nmi³/s² (398 600 km³/s²)	$\partial(\Delta V_2)/\partial r_p$	0 s^{-1}

3.2 Simplification

It is possible to simplify the condition of Eq(12). First, note from Eq(9) that ΔV_2 has no dependence on the post-aerocapture periapsis radius (i.e., $\partial(\Delta V_2)/\partial r_p = 0$), permitting the last term of Eq(12) to be dropped. Second, note that the argument in Section 3.1 assumed that apoapsis and periapsis altitudes are monotonically decreasing functions of bank angle. As a result, the perturbation represented by the derivative in Eq(10) is always in a region where $r_a > r_{aT}$, and the bottom portion of Eq(8) can be used. Third, note from Table 2 that $\partial(\Delta V_1)/\partial r_a$ is two orders of magnitude smaller than the other nonzero ΔV derivatives. This occurs because r_p and r_{pT} differ by a relatively small amount (only 10% in Table 2), and if they were equal, Eq(6) shows that $\partial(\Delta V_1)/\partial r_a$ would vanish. In other words, as long as the post-aerocapture periapsis radius is

comparable to the periapsis radius of the target orbit (as is often the case), ΔV_1 is not particularly sensitive to the achieved post-aerocapture apoapsis radius. Making these simplifications, plus substituting r_{aT} for r_a because the equivalence condition is, by definition, applied where $r_a = r_{aT}$, yields Eq(13):

$$-\frac{\sqrt{2\mu}}{2\left(r_{aT}+r_p\right)^{3/2}}\sqrt{\frac{r_{aT}}{r_p}}\frac{dr_p}{d\phi} < -\frac{\sqrt{2\mu}}{2}\frac{\sqrt{r_{pT}}}{\sqrt{r_{aT}}\left(r_{aT}+r_{pT}\right)^{3/2}}\frac{dr_a}{d\phi} \tag{13}$$

Simplifying further yields Eq(14), a requirement on the ratio between the two numerical derivatives that can be computed prior to a trajectory run (e.g., as in fig. 8). In the example case of Table 2, this ratio is -39.7/-23.1 = 1.72. The right side of Eq(14), which evaluates to 1.13 for the values in Table 2, indicates correctly again that the equivalence condition is satisfied (i.e., that 1.72 > 1.13 is true) and, in this scenario, apoapsis targeting is equivalent to ΔV minimization. It is worth noting that if $r_p \approx r_{pT}$, then the right side of Eq(14) becomes simply the ratio between the target apoapsis and periapsis radii.

$$\frac{dr_a/d\phi}{dr_p/d\phi} > \frac{r_{aT}}{\sqrt{r_p r_{pT}}}\left(\frac{r_{aT}+r_{pT}}{r_{aT}+r_p}\right)^{3/2} \tag{14}$$

Importantly, Eq(14) now provides a tool with which to efficiently answer the question of whether any combinations of target periapsis and apoapsis can produce a scenario in which apoapsis targeting is not identical to (i.e., less optimal than) ΔV minimization. This occurs whenever the condition of Eq(14) is violated.

To initiate this analysis, we first compute the $(dr_a/d\varphi)$ / $(dr_a/d\varphi)$ ratio on the left side of Eq(14) at each bank angle in figure 8. Next, to compute the right side of Eq(14) as a function of bank angle, we recognize that each bank angle is associated with a unique apoapsis. This apoapsis becomes r_a in Eq(14). The periapsis (r_p) in Eq(14) is the corresponding periapsis (e.g., directly from the lower plot of fig. 8). For periapsis altitudes comparable to the radius of the planet, the right side is a weak function of periapsis target (r_{pT}); for convenience, this is selected here as 3543.9 nmi (6563.3 km), corresponding to a 100-nmi (185-km) altitude. As a result, we now have both the left and right sides of Eq(14) as a function of the NPC-selected bank angle and can plot them as such. Since apoapsis altitude is a monotonically decreasing function of bank angle, the *x*-axis of such a plot can be easily changed to display apoapsis altitude; this is the graph shown in figure 9.

Figure 9 shows how the values of the left and right sides of Eq(14) change with target apoapsis altitude. At apoapsis altitudes where the left-side line is higher than the right-side line (i.e., to the right of the red vertical line), both apoapsis targeting and ΔV minimization are equivalent. Notice from the figure that the crossover for this particular scenario occurs at 188.4 nmi (348.9 km), which agrees with the empirical observation that a 229-nmi (425-km) apoapsis target results in equivalence between apoapsis targeting and ΔV minimization. However, the major implication of figure 9 is that target apoapses below 188.4 nmi (348.9 km) should theoretically benefit from a ΔV minimization algorithm. This will be tested next.

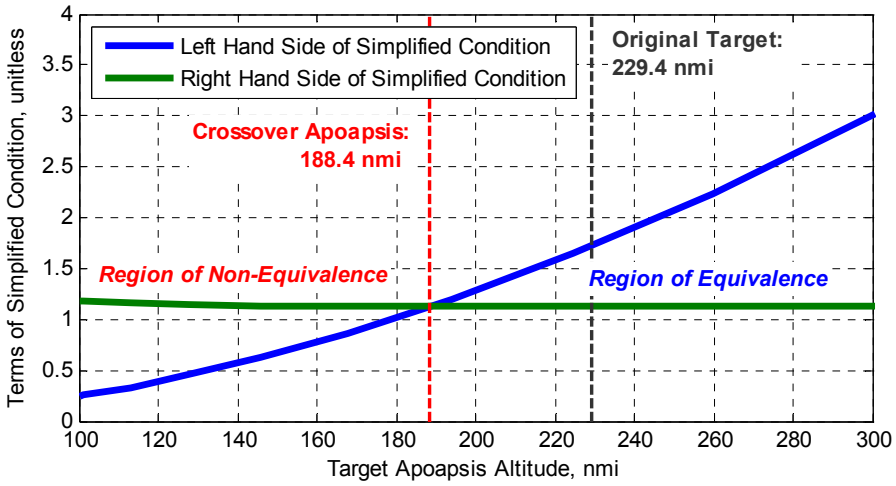

Figure 9. Left and right sides of the simplified equivalence condition (Eq[14]) plotted as a function of target (and achieved) apoapsis altitude, assuming a 100-nmi (185.2-km) target periapsis altitude.

Before continuing, it is worth emphasizing that figure 9 can be produced in advance (or at least at the very first time step) of entry. All the data used to produce it was gathered from the initial NPC prediction of achieved apoapsis and periapsis altitudes as a function of bank angle. The implication of this for future development is that the most suitable technique (apoapsis targeting or ΔV minimization) can be easily selected prior to execution of the aerocapture maneuver.

3.3 Verification: An Example of Non-equivalence

As mentioned in Section 3.2, for the Orion lunar return test case, target apoapsis altitudes below 188.4 nmi (348.9 km) should theoretically benefit from the ΔV minimization algorithm. This is tested here with a target orbit of 108.1 nmi (200.3 km).

Figure 10, which is similar to figure 7, illustrates the bank angles commanded by the two competing algorithms when using this new target. Unlike figure 7, the two bank angle profiles no longer align. As shown in Table 3, the apoapsis targeting technique initially commands a -45.4-deg bank angle, whereas the ΔV minimization technique initially commands a bank angle of -41.1 deg. As expected, both angles are held approximately constant until the first bank reversal. As the peak deceleration is passed, the vehicle gradually loses control authority and bank angle commands become more sensitive to differences between the internal PredGuid predictor simulation and the actual SORT simulation. Both NPCs deactivate about 3.5 min into the trajectory.

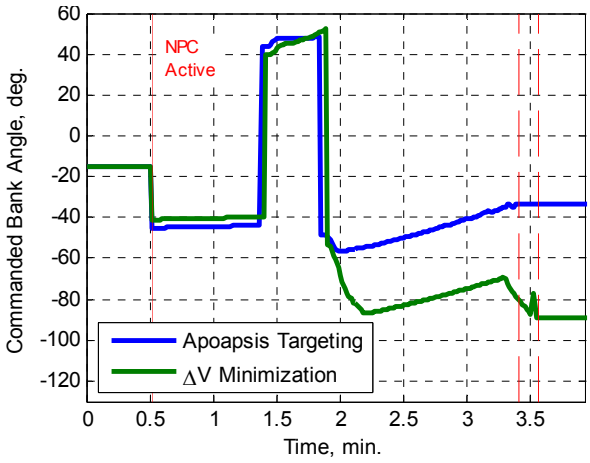

Figure 10. Comparison of commanded bank angle between apoapsis targeting and ΔV minimization for a 108.1-nmi (200.3-km) circular target orbit.

Despite the seemingly small 4.3-deg difference between the two commanded bank angles, the effect on the vehicle exit state is significant. As Table 3 shows, the apoapsis targeting algorithm does achieve the target apoapsis of 108.1 nmi (200.3 km) (the algorithm misses by just 208 ft [63.4 m]). The table also shows that the ΔV minimization algorithm misses the target apoapsis by a greater amount of 0.6 nmi (1.2 km). Thus, the apoapsis targeting technique requires virtually no apoapsis cleanup ΔV (just 0.06 fps [0.02 m/s]), while the ΔV minimization technique requires a 1.15 fps (0.35 m/s) burn. Much more significant, however, is the 88.8 nmi (164.5 km) difference in periapsis between the two algorithms. As a result, the periapsis raise burn requires a dramatically higher ΔV for the apoapsis targeting technique (802.62 fps [244.64 m/s]) than for the ΔV minimization technique (619.89 fps [188.94 m/s]). In this case, since the ΔV minimization technique considered the ΔV trades when deciding upon bank angle, a 23% ΔV savings results.

Table 3. Comparison of NPC Technique Performance to 108.1-nmi (200.3-km) Orbit.

	Apoapsis Targeting Technique	ΔV Minimization Technique
Initial NPC Bank Angle (φ)	-45.36°	-41.06°
Post-aerocapture Apoapsis Altitude	108.1 nmi (200.2 km)	107.5 nmi (199.1 km)
Post-aerocapture Periapsis Altitude	-305.8 nmi (-566.3 km)	-217.0 nmi (-401.8 km)
Post-aerocapture Apoapsis Radius (r_a)	3552.0 nmi (6578.3 km)	3551.4 nmi (6577.2 km)
Post-aerocapture Periapsis (r_p)	3138.1 nmi (5811.8 km)	3227.0 nmi (5976.3 km)
Periapsis Raise ΔV (ΔV_1)	802.62 ft/s (244.64 m/s)	619.89 ft/s (188.94 m/s)
Apoapsis Cleanup ΔV (ΔV_2)	0.06 ft/s (0.02 m/s)	1.15 ft/s (0.35 m/s)
Total ΔV	**802.68 ft/s (244.66 m/s)**	**621.04 ft/s (189.29 m/s)**

4. Monte Carlo Performance

To verify the robustness of both the apoapsis targeting and ΔV minimization methods, Monte Carlo simulations are executed. Results of 2000-case simulations are given in figures 11 and 12. Input dispersions are derived primarily from early estimates for the Orion vehicle,[36] with atmospheric dispersions drawn from nominal small-scale perturbations of the Earth GRAM [Global Reference Atmosphere Model] 07 [37] on February 2, 2010. Note that this is the only time in this study in which GRAM 07 is used as an atmosphere model in the SORT simulation; earlier simulation results are based on use of the 1976 U.S. Standard Atmosphere in both the PredGuid predictor and the SORT simulation. Implemented dispersions are summarized in Table 4.

Table 4. Non-atmospheric Monte Carlo Dispersions. *Variables are uniformly distributed except for those with a 3σ indicator, which are distributed normally.*

Variable	Distribution Range
Init. Longitude	-116.50 ± 0.20 deg
Init. Geodetic Latitude	-46.67 ± 0.20 deg
Init. Geodetic Altitude	400,000 ± 500 ft
Init. Inertial Velocity	36,150 ± 90 ft/s (3σ)
Init. Inertial Flt. Path Ang.	-5.91 ± 0.01 deg (3σ)
Init. Inertial Azimuth	0.00 ± 0.05 deg
Vehicle Mass	19804.7 ± 613.9 lbm
Lift Coeff. Multiplier	1.00 ± 0.15 (3σ)
Drag Coeff. Multiplier	1.00 ± 0.15 (3σ)

Figure 11 shows histograms of Monte Carlo results associated with the original 229 nmi (425 km) circular target orbit. The upper plot shows the total ΔV (the sum of the periapsis raise burn and the apoapsis cleanup ΔV values) if the apoapsis targeting guidance is used, and the lower plot shows the total ΔV if the ΔV minimization guidance is used. Recall that in this scenario, the

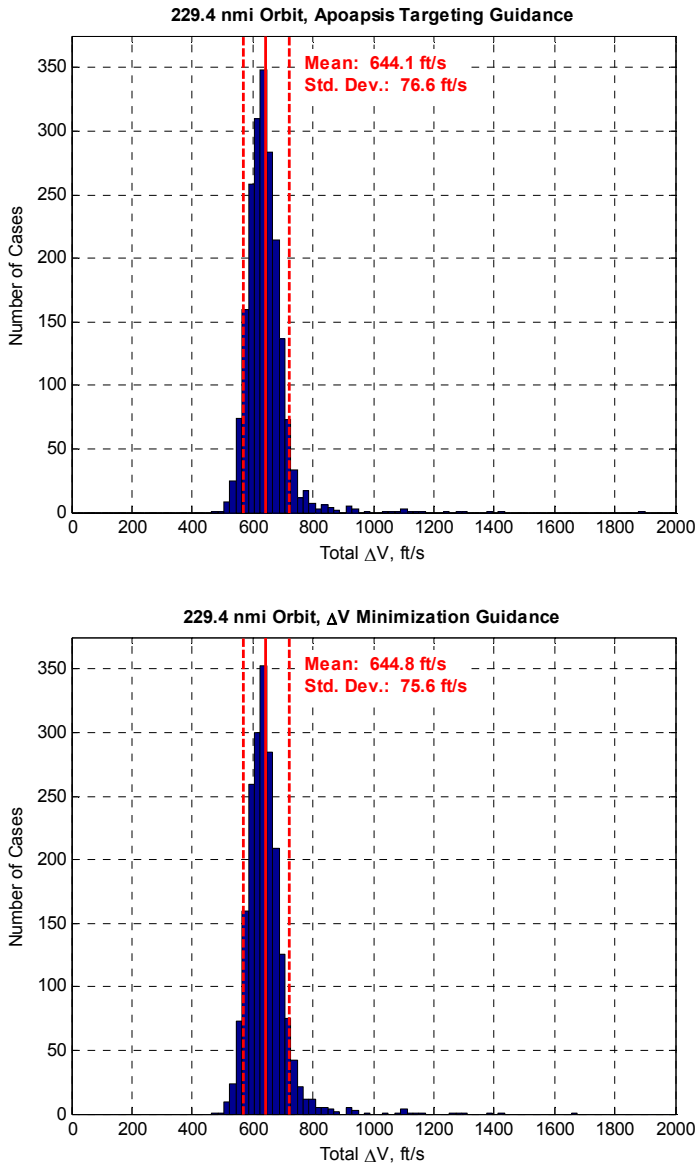

Figure 11. Comparison of ΔV Monte Carlo outputs between apoapsis targeting and ΔV minimization for the 229.4-nmi (424.9-km) orbit.

nominal cases of figures 5 and 6 showed that both guidance algorithms should choose the same bank angle and result in the same exit conditions and ΔV. This is reflected in the Monte Carlo results: The mean of both distributions agree to within 0.7 fps (0.2 m/s, or 0.1%), and the standard deviations agree to within 1.0 fps (0.3 m/s, or 1.3%).

Figure 12 shows histograms of Monte Carlo results associated with the lower 108.1-nmi (200.3-km) target circular orbit. In this scenario, the results show significant differences. The mean ΔV for the apoapsis targeting guidance is 204.2 fps (62.2 m/s, or 34%) higher than for the ΔV minimization guidance. This is expected, given the nominal result from the non-equivalence verification of Section 3.3. It is also notable that the distribution for the ΔV minimization guidance is more tightly contained around the mean, with a standard deviation 24% smaller than the apoapsis targeting results.

Thus, this Monte Carlo analysis serves to (1) confirm the observation made in Section 3 that apoapsis targeting is conditionally equivalent to ΔV minimization; and (2) illustrate that the benefits of ΔV minimization guidance in scenarios of non-equivalence can extend to both the mean and the standard deviation of the post-aerocapture ΔV.

5. Summary and Implications

This paper has explored a basic question that arises in the development of aerocapture numerical predictor-corrector guidance algorithms: Why target apoapsis? The more fundamental objective of the aerocapture maneuver is to minimize the total ΔV required to insert into the final target orbit.

This paper conveys both good news and bad news for the traditional apoapsis targeting method. The bad news is that situations clearly exist in which apoapsis targeting results in excessive ΔV expenditure (e.g., see Table 3 or fig. 12). The surprising good news, however, is

that in many scenarios (for the test case in this paper, target apoapsis altitudes higher than 188.4 nmi [348.9 km]) apoapsis targeting is equivalent to ΔV minimization. More importantly, though, this paper has shown that the condition under which equivalence occurs can be easily evaluated prior to entry.

5.1 Sample Guidance Selection Procedure

By definition, ΔV minimization guidance should always be at least as ΔV-optimal as apoapsis targeting. Thus, from a ΔV performance perspective, ΔV minimization guidance should always be preferred. However, in order to operate, the ΔV minimization algorithm employs a one-dimensional (1-D) minimization technique (in this implementation, golden section search, although this can be revisited in future versions), which will always require more function evaluations than a 1-D search or targeting problem. Whether these additional function evaluations can be tolerated depends on the capabilities of on-board flight computers for future missions.[§] In the event that a trade must be made between computational speed and ΔV performance, this paper provides the basis for a decision procedure.

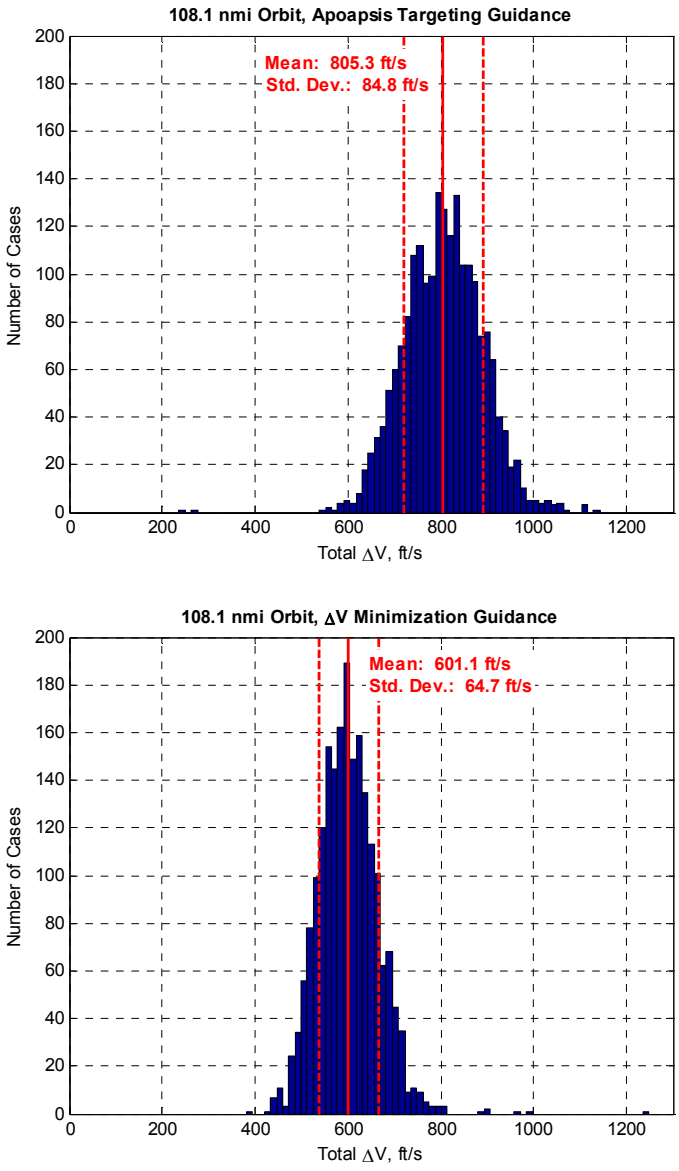

Figure 12. Comparison of ΔV Monte Carlo outputs between apoapsis targeting and ΔV minimization for the 108.1-nmi (200.3-km) orbit.

Figure 13 shows a five-step summary procedure for repeating the analysis of this paper for general scenarios. In Steps 1 and 2, the problem is defined in terms of initial conditions, simulation assumptions, and a target final orbit. Steps 3 and 4 mirror the analysis of Section 3 by computing the apoapsis and periapsis altitudes and derivatives as a function of bank angle. Step 5 involves evaluating the equivalence condition (derived in Section 3.2) based on the derivatives and altitudes computed in Steps 3 and 4. It is important to reiterate that the equivalence condition derived in this paper assumes that apoapsis and periapsis altitude each monotonically decrease with the chosen bank

[§]A potential area for future investigation would involve verifying that the ΔV minimization guidance is still ΔV-competitive if called less frequently, thereby reducing computational demands.

angle. While this makes intuitive sense, it should be verified on a case-by-case basis before using the condition.**

The advantage to the procedure of figure 13 is that if the NPC simulation well reflects reality (or the external simulation), it can be conducted once by the on-board NPC prior to the beginning of entry or the beginning of an entry simulation. Based on the results of the procedure, a user or the NPC itself could choose whether to execute apoapsis targeting guidance or the more computationally intensive (but possibly lower ΔV) ΔV minimization guidance.

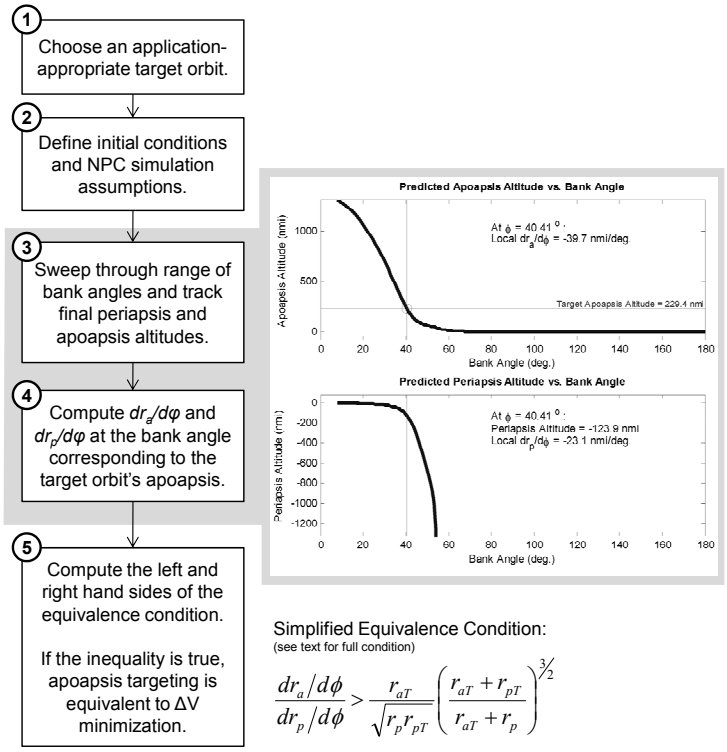

Figure 13. Sample apoapsis targeting vs. ΔV minimization decision procedure. *Note that Step 5 assumes that apoapsis and periapsis altitude monotonically decrease with bank angle.*

5.2 Limitations and Future Work

Strictly speaking, the main results of this work are applicable only to aerocapture guidance algorithms that iterate on one time-invariant bank angle. While this approach is common, it may be possible to improve ΔV performance by allowing the NPC to solve for a time-varying bank angle. This would require a corrector with a more sophisticated multidimensional search technique (and an increase in computational power); and if an equivalence condition exists, it would be more complex than in Eq(12) or Eq(14).

A second limitation to acknowledge is the fact that because PredGuid considers lateral logic independently from longitudinal logic, plane change ΔV cannot be predicted or optimized even by the ΔV minimization guidance algorithm. In effect, the NPC's assumption is that the lateral logic is sufficient to make any plane change burn unnecessary. Integrating lateral logic into the predictor to allow prediction of plane change ΔV may be a worthwhile area of future study.

Additional future work involves applying the equivalence condition derived here for a wide variety of entry condition test cases. Additional tests for geosynchronous orbit return or AFE-like LEO entry conditions would be applicable to future uncrewed aerocapture tests at Earth. Test simulations for incoming hyperbolic trajectories at Mars are also likely, and hyperbolic test cases at other planets or moons may be warranted. Overall, it is hoped that the conditional equivalence of apoapsis targeting and ΔV minimization highlighted in this paper becomes a significant consideration in any future design and development of aerocapture NPC guidance.

**If the character of the graph is found not to be monotonically decreasing, a new condition can be derived based on logic similar to that of Section 3.2.

6. References

[1]Munk, M.M. and Moon, S.A., "Aerocapture Technology Development Overview," IEEEAC Paper #1447, IEEE Aerospace Conference, Big Sky, 1-8 March 2008.

[2]Hall, J., "An Overview of the Aerocapture Flight Test Experiment (AFTE)," AIAA 2002-4621, Atmospheric Flight Mechanics Conference, Monterey, 5-8 Aug. 2002.

[3]Anderson, D.J., Pencil, E., et. al., Liou, L, Dankanich, J., Munk, M.M., and Kremic, T., "The NASA In-Space Propulsion Technology Project, Products, and Mission Applicability," IEEEAC Paper #1176, IEEE Aerospace Conference, Big Sky, 7-14 March 2009.

[4]Hall, J.L., Noca, M.A., and Bailey, R.W., "Cost-Benefit Analysis of the Aerocapture Mission Set," *Journal of Spacecraft and Rockets*, Vol. 42, No. 2, March 2005. pp. 309-320.

[5]Hubbard, G.S., Lunine, J., et. al., "Solar System Exploration," JPL D-35618, NASA Jet Prop. Lab, Pasadena, 15 Sept. 2006.

[6]Drake, B.G., Hoffman, S.J., and Beaty, D.W., "Human Exploration of Mars Design Reference Architecture 5.0," IEEEAC Paper #1205, IEEE Aerospace Conference, Big Sky, 6-13 March 2010.

[7]Hoffman, S.J. and Kaplan, D.I. (ed.), "Human Exploration of Mars: The Reference Mission of the NASA Mars Exploration Study Team," NASA SP-6107, NASA Johnson Space Center, Houston, July 1997.

[8]Drake, B.G., (ed.), "Reference Mission 3.0, Addendum to the Human Exploration of Mars: The Reference Mission of the NASA Mars Exploration Study Team," NASA SP-6107-ADD, NASA Johnson Space Center, Houston, June 1998.

[9]Zubrin, R.M., Baker, D.A., and Gwynne, O., "Mars Direct: A Simple, Robust, and Cost Effective Architecture for the Space Exploration Initiative," AIAA 1991-0329, AIAA 29th Aerospace Sciences Meeting, Reno, 7-10 Jan. 1991.

[10]Zubrin, R., *The Case for Mars,* Free Press, New York, 1996, Chap. 1.

[11]Christian, J.A., Wells, G., Lafleur, J., Verges, A., and Braun, R.D., "Extension of Traditional Entry, Descent, and Landing Technologies for Human Mars Exploration," *Journal of Spacecraft and Rockets*, Vol. 45, No. 1, Jan. 2008. pp. 130-141.

[12]James, B.F., "NASA Office of the Chief Technologist Crosscutting Capability Demonstrations Division Technology Demonstration Missions Program," Acquisition Notice Posting, Solicitation Number NNH10CC001L, Greenbelt, 25 May 2010.

[13]Braun, R., "Office of the Chief Technologist Town Hall Meeting," Presentation, 25 May 2010. URL: http://www.nasa.gov/pdf/457884main_OCT_town_hall_rev4.pdf [20 July 2010].

[14]Walberg, G.D., "A Survey of Aeroassisted Orbit Transfer," *Journal of Spacecraft*, Vol. 22, No. 1, Jan. 1985. pp. 3-18.

[15]Mease, K.D., Weidner, R.J., Kechichian, J., Wood, L.J., and Cruz, M.I., "Aerocapture: Guidance, Navigation, and Control," AIAA 1982-1381, Atmospheric Flight Mechanics Conference, San Diego, 9-11 Aug. 1982.

[16]Kechichian, J., Cruz, M.I., Rinderle, E.A., and Vinh, N.X., "Optimization and Closed-Loop Guidance of Drag-Modulated Aeroassisted Orbital Transfer," AIAA 1983-2093, Atmospheric Flight Mechanics Conference, Gatlinburg, 15-17 Aug. 1983.

[17]Gamble, J.D., Cerimele, C.J., Moore, T.E., and Higgins, J., "Atmospheric Guidance Concepts for an Aeroassist Flight Experiment," *The Journal of the Astronautical Sciences*, Vol. 36, Nos. 1-2, Jan. 1988. pp. 45-71.

[18]Rousseau, S., Perot, E., Graves, C., Masciarelli, J.P., and Queen, E., "Aerocapture Guidance Algorithm Comparison Campaign," AIAA 2002-4822, AIAA/AAS Astrodynamics Specialist Conference, Monterey, 5-8 Aug. 2002.

[19]Cerimele, C.J. and Gamble, J.D., "A Simplified Guidance Algorithm for Lifting Aeroassist Orbital Transfer Vehicles," AIAA 1985-0348, AIAA 23rd Aerospace Sciences Meeting, Reno, 14-17 Jan. 1985.

[20]Masciarelli, J., "Aerocapture Guidance Algorithm Development and Testing," Paper D8P3, NASA Science Technology Conference, College Park, 19-21 June 2007.

[21]Powell, R.W., "Numerical Roll Reversal Predictor Corrector Aerocapture and Precision Landing Guidance Algorithms for the Mars Surveyor Program 2001 Missions," AIAA 1998-4574, Atmospheric Flight Mechanics Conf., Boston, 10-12 Aug. 1998.

[22]Casoliva, J. and Mease, K.D., "Analytical Atmospheric Guidance for Aerocapture," AAS 07-308, AAS/AIAA Astrodynamics Specialist Conference, Mackinac Island, 19-23 Aug. 2007.

[23]Cruz, M.I., "Aerocapture Vehicle Mission Design Concepts for the Inner and Outer Planets," AAS 79-115, AAS/AIAA Astrodynamics Specialist Conference, Provincetown, 25-27 June 1979.

[24]Hill, O., "An Adaptive Guidance Logic for an Aeroassisted Orbital Transfer Vehicle," AAS 83-357, AAS/AIAA Astrodynamics Specialist Conference, Lake Placid, 22-25 Aug. 1983.

[25]Rehder, J.J., "A Linear Feedback Guidance Law for an Aeromaneuvering Orbit-to-Orbit Shuttle," AAS 75-065, AAS/AIAA Astrodynamics Specialist Conference, Nassau, 28-30 July 1975.

[26]Spathopoulos, T., "Ein Verfahren zur Lenkung des Synergetischen Bahndrehmanövers," Doctoral Dissertation, Dept. of Mechanical and Electrical Engineering, Technical University Munich, Munich, 1975.

[27]Putnam, Z.R., Barton, G.H., and Neave, M.D., "An Entry Trajectory Design Methodology for Lunar Return," AIAA 2009-5773, AIAA Guidance, Navigation, and Control Conference, Chicago, 10-13 Aug. 2009.

[28]Hoelscher, B.R., "Orion Entry, Descent, and Landing Simulation," AIAA 2007-6428, AIAA Guidance, Navigation, and Control Conference, Hilton Head, 20-23 Aug. 2007.

[29]DiCarlo, J.L., "Aerocapture Guidance Methods for High Energy Trajectories," M.S. Dissertation, Dept. of Aeronautics and Astronautics, Massachusetts Institute of Technology, Cambridge, 2003.

[30]Bairstow, S.H., "Reentry Guidance with Extended Range Capability for Low L/D Spacecraft," M.S. Dissertation, Dept. of Aeronautics and Astronautics, Massachusetts Institute of Technology, Cambridge, 2006.

[31]Rea, J.R. and Putnam, Z.R., "A Comparison of Two Orion Skip Entry Guidance Algorithms," AIAA 2007-6424, AIAA Guidance, Navigation, and Control Conference, Hilton Head, 20-23 Aug. 2007.

[32]Bairstow, S.H. and Barton, G.H., "Orion Reentry Guidance with Extended Range Capability using PredGuid," AIAA 2007-6427, AIAA Guidance, Navigation, and Control Conference, Hilton Head, 20-23 Aug. 2007.

[33]Fuhry, D.P., "A Design Study of Onboard Navigation and Guidance during Aerocapture at Mars," M.S. Dissertation, Dept. of Aeronautics and Astronautics, Massachusetts Institute of Technology, Cambridge, 1988.

[34]Wahbah, M.M., Berning, M.J., and Choy, T.S., "Simulation of Airplane and Rocket Trajectories," *NASA Tech Briefs,* Vol. 11, No. 7, July 1987, p. 62.

[35]Morth, R., *Reentry Guidance for Apollo,* Vol. 1, MIT Instrumentation Laboratory, Cambridge, 1966, Chaps. 4,5.

[36]Tigges, M., Crull, T., Rea, J., and Johnson, D., "Numerical Skip-Entry Guidance," AAS 07-076, 30th Annual AAS Guidance and Control Conference, Breckenridge, 3-7 Feb. 2007.

[37]Justus, C.G. and Leslie, F.W., "The NASA MSFC Earth Global Reference Atmospheric Model – 2007 Version," NASA TM-2008-215581, NASA Marshall Space Flight Center, Nov. 2008.

REPORT DOCUMENTATION PAGE

Form Approved
OMB No. 0704-0188

1. AGENCY USE ONLY *(Leave Blank)*	2. REPORT DATE	3. REPORT TYPE AND DATES COVERED
	August 2011	Technical Memorandum

4. TITLE AND SUBTITLE
The Conditional Equivalence of ΔV Minimization and Apoapsis Targeting in Numerical Predictor-Corrector Aerocapture Guidance

5. FUNDING NUMBERS

6. AUTHOR(S)
Jarret M. Lafleur*

7. PERFORMING ORGANIZATION NAME(S) AND ADDRESS(ES)
Lyndon B. Johnson Space Center
Houston, Texas 77058

8. PERFORMING ORGANIZATION REPORT NUMBERS
S-1103

9. SPONSORING/MONITORING AGENCY NAME(S) AND ADDRESS(ES)
National Aeronautics and Space Administration
Washington, DC 20546-0001

10. SPONSORING/MONITORING AGENCY REPORT NUMBER
TM-2011-216156

11. SUPPLEMENTARY NOTES
*NASA Johnson Space Center, Houston

12a. DISTRIBUTION/AVAILABILITY STATEMENT
Unclassified/Unlimited
Available from the NASA Center for AeroSpace Information (CASI)
7115 Standard
Hanover, MD 21076-1320 Category: 13

12b. DISTRIBUTION CODE

13. ABSTRACT *(Maximum 200 words)*

Interest in aerocapture, a maneuver in which a spacecraft dives into the atmosphere of a planet for nearly propellantless capture into planetary orbit, has grown steadily in recent years. One key element required to execute this maneuver is an appropriate guidance algorithm for the atmospheric phase of flight. A popular algorithm choice has been the numerical-predictor corrector (NPC), which typically iterates on a time-invariant bank angle to target apoapsis of the desired final orbit. This paper introduces the idea of using the NPC to select the bank angle that instead minimizes the sum of periapsis-raise ΔV and apoapsis-cleanup ΔV, and demonstrates the surprising finding that the two approaches are equivalent under a certain analytic condition. This condition is derived and then applied to correctly predict a scenario in which apoapsis targeting produces a suboptimal ΔV. This scenario is simulated, and the ΔV minimization algorithm is shown to reduce the required ΔV by 23%. Monte Carlo simulations confirm both the scenarios of equivalence and non-equivalence, and an automatable procedure is outlined that a user can execute prior to simulating or flying a trajectory to determine whether apoapsis targeting is ΔV optimal or whether a ΔV minimization algorithm is required.

14. SUBJECT TERMS	15. NUMBER OF PAGES	16. PRICE CODE
trajectories; trajectory analysis; astrodynamics; trajectory control; trajectory optimization; flight mechanics; trajectory planning; flight simulation	32	

17. SECURITY CLASSIFICATION OF REPORT	18. SECURITY CLASSIFICATION OF THIS PAGE	19. SECURITY CLASSIFICATION OF ABSTRACT	20. LIMITATION OF ABSTRACT
Unclassified	Unclassified	Unclassified	Unlimited